

# Size and Quality of Quantum Mechanical Data Sets for Training Neural Network Force Fields for Liquid Water

Márcio S. Gomes-Filho,<sup>\*,†</sup> Alberto Torres,<sup>‡</sup> Alexandre Reily Rocha,<sup>¶</sup> and Luana S.  
Pedroza<sup>\*,†</sup>

<sup>†</sup>*Centro de Ciências Naturais e Humanas, Universidade Federal do ABC, Santo André,  
09210-580, São Paulo, Brazil*

<sup>‡</sup>*Instituto de Física, Universidade de São Paulo, São Paulo, 05508-090, Brazil*

<sup>¶</sup>*Institute of Theoretical Physics, São Paulo State University, Campus São Paulo, 01140-070,  
Brazil*

E-mail: marcio.sampaio@ufabc.edu.br; l.pedroza@ufabc.edu.br

## Abstract

Molecular dynamics simulations have been used in different scientific fields to investigate a broad range of physical systems. However, the accuracy of calculation is based on the model considered to describe the atomic interactions. In particular, *ab initio* molecular dynamics (AIMD) has the accuracy of density functional theory (DFT), and thus is limited to small systems and relatively short simulation time. In this scenario, Neural Network Force Fields (NNFF) have an important role, since it provides a way to circumvent these caveats. In this work we investigate NNFF designed at the level of DFT to describe liquid water, focusing on the size and quality of the training data-set considered. We show that structural properties are less dependent on the size of the training data-set compared to dynamical ones (such as the

diffusion coefficient), and a good sampling (selecting data reference for training process) can lead to a small sample with good precision.

## Introduction

Molecular dynamics simulations have been used in different scientific fields to investigate a broad range of physical systems, such as thermodynamic properties of liquids, physico-chemical aspects of interfaces and biomolecules.<sup>1-3</sup> Its success relies on a number of factors, for example, the functional form assigned to describe inter- and intra-atomic interactions, the parametrization procedure (obtaining the potential parameters), and the quality of data employed - experimental or *ab initio* one.<sup>4,5,5-10</sup> Most of the classical potentials are physically and/or chemically motivated, in which a simple analytical functional form is usually considered such as the Lennard-Jones potential.<sup>11</sup> As a consequence, transferability, and accuracy are a common issue in this area of research.<sup>5,7,12</sup>

In the particular case of water, many classical empirical models have been proposed to describe its properties. Although some classical models, such as the MB-Pol, provide fairly good results for water,<sup>13-15</sup> there is no single water model capable of exactly reproducing all experimental results.<sup>16</sup> In fact, over the last decades, there has been an advance in the understanding of the properties of water both by theory/simulations as experimentally. However, there are still some of its properties which are not yet fully understood. For example, the microscopic origin of the water anomalies.<sup>17</sup> From a microscopic point of view, the quantum nature of the hydrogen bond network, the interplay between short and long range interactions and nuclear quantum effects make the liquid water intrinsically difficult to be modelled. In this way, based on the nature of the phenomena that governs the physical and chemical properties of liquid water, first principles simulations seem to be the most appropriate choice, since they have, by construction, an accurate predictive potential. These types of simulations have the advantage of forgoing the requirement for a model or the parametrization of any experimental data. In particular, *ab initio* molecular dynamics (AIMD) allows one to obtain the energy/forces on-the-fly by a quantum mechanical method such as density

functional theory (DFT)<sup>18</sup> at each time step. The caveat is the limitation to small system sizes and short simulations time.<sup>5</sup> Furthermore, the quality of the AIMD simulations is closely determined by the chosen exchange-correlation (xc) functional.<sup>19–21</sup>

In this scenario, machine learning (ML) potentials - also known as ML force fields<sup>12</sup> - have introduced a paradigm change as one can now combine the quantum accuracy of AIMD with computational efficiency of empirical interatomic models. This allows one to simulate large systems for long time with *ab initio* accuracy. These methods have been recognized as promising alternatives to underline new physical phenomena and aid in materials-discovery processes.<sup>6,12,22–30</sup> In particular, the microscopic comprehension of bulk water can benefit from computer simulations based on ML potentials.<sup>26,31–34</sup>

Many different ML methods have been used to construct these ML-based potentials, for example artificial neural networks,<sup>4,6,8,35–40</sup> kernel-based methods,<sup>30,41</sup> gaussian approximation potentials,<sup>42,43</sup> and atomic cluster expansion.<sup>44</sup> In particular, deep Neural Networks (NN) approaches have been shown to be a versatile tool able to produce accurate Force Fields (FF) trained with DFT calculations.<sup>6,7,26</sup> The successful/accuracy of ML potentials is directly related to the quality and size of the training data-set employed.<sup>12,45,46</sup> Usually, deep NN approaches require a large amount of data, but typically provide a high accuracy.<sup>4,23,47</sup> Therefore, having a deep NN potential trained with less DFT data reference is a very important issue,<sup>4,48</sup> since the DFT calculation of the reference data-set is highly computational demanding.

In this work we investigate deep NNFF designed at the level of DFT to describe liquid water, focusing on the size and quality of the training data-set considered. Here, we chose to investigate the *ab initio* training data-set based on the SCAN functional,<sup>49</sup> since it has shown some promising results for water.<sup>26,31,50–56</sup> We show that correctly sampling the data (selecting reference data for the training process) is a crucial step, and devising a method to efficiently obtain uncorrelated structures that provide a good distribution over the phase space allows one to significantly reduce the amount of data and the size of the NN required to have accurate NNFF. As a result we also show that the structural properties are less dependent on the size of the training data-set compared

to dynamical ones (e.g, the diffusion coefficient.)

## Methods

### Computational Details

A crucial step in the development of the NN force field was to carefully select the bulk water configurations, which included configurations with long and short OH bonds before computing the DFT energies and forces used in the training process. The protocol to obtain those configuration was: (i) the selected configurations were obtained considering nuclear quantum effects (NQE) in classical MD simulations by carrying out partially adiabatic centroid molecular dynamics (PACMD)<sup>57</sup> simulations using a flexible water model (q-TIP4P/F force field<sup>58</sup>) for a system composed by 64 water molecules; (ii) good phase space sampling was obtained by performing simulations with different temperatures ( $T = 300$  and  $600$  K) and densities ( $\rho = 0.88, 1.0$ , and  $1.2$  g/cm<sup>3</sup>), and (iii) selecting uncorrelated configurations (i.e, geometrical structures) through radial distribution functions, choosing those that maximized the Jensen-Shannon distance.<sup>59</sup> In this way, a broad range of intra- and intermolecular geometric configurations were present in the training set.<sup>26</sup>

For each set of PACMD simulation (different  $T$  and  $\rho$ ), the geometries were collected every 100 fs from a total simulation time of 1 ns ( $10^4$  configurations). After geometric selection criteria, the number of configurations were 5000 (1000) for  $T = 300$  K (600 K), which resulted in  $18 \times 10^3$  snapshots. Then, for each configuration we performed a single point DFT calculation to obtain the total energies and forces. In our particular case, the reference data were obtained using the Vienna *Ab initio* Simulation Package (VASP)<sup>60</sup> and SCAN functional.<sup>49</sup> The plane wave basis was set up to an energy cutoff of 1600 eV (118 Ry), and the core-valence interaction was treated by the projected augmented wave (PAW) method.<sup>61</sup> Note that all DFT calculations are completely independent from each other, and thus can be performed separately.

## Training process

A crucial point in the design of neural network-trained force fields is to determine the minimum size of the training set to obtain *ab initio* quality results. In this way, we trained our NNFFs using a randomly selected subset of the training data set ranging from 10% to 100% of the total data set.

We first selected 90% of the configurations as the training set and 10% as the testing set for assessment, which means 16200 (training) e 1800 (testing) structures. It is important to emphasize that the data used in the training is  $n_{data} = n_{energy} + n_{force}$ . We have one energy value per configuration (64 H<sub>2</sub>O),  $n_{energy} = 16200$ . Whereas for force, there are three components,  $\{f_x, f_y, f_z\}$ , for each atom, i.e  $n_{force} = 16200 \times 3 \times 192$ . Therefore, we have  $n_{data} = 9347400$  training data.

On the other hand, in order to avoid over-fitting (when the model performs worse on the testing data than on their training set) the number of fitted parameters,  $n_{parm}$ , cannot be larger than the number of training data points. In this work, we chose  $n_{data}/n_{parm}$  to be at least 8. Note that in order to avoid over-fitting one can either increase the size of the training set or reduce the number of layers and/or the number of neurons of each layer.<sup>6,8,62</sup>

Therefore, we scaled down the neural network in order to keep the total number of fitted parameters in the same proportion. For example, the NN topology (the number of hidden layers is 4 and the number of neurons in each layer) is set to (32, 16, 4, 2) and (320, 160, 32, 16) for the 10% and 100% case, respectively.

We used the current version of the DeePMD-kit code<sup>8</sup> to generate deep neural network potentials for bulk water based on the SCAN functional. In particular, we use the Deep Potential-Smooth Edition descriptor, where the full relative coordinates are used to build the descriptor.<sup>6,63</sup> The number of hidden layers is kept fixed, and the hyperbolic tangent was used as an activation function in the hidden layers. The loss function was minimized with the Adam stochastic gradient descent method,<sup>64</sup> composed by the mean squared errors of the energies and forces with a starting and stopping learning rate equal to  $10^{-3}$  and  $3.51 \times 10^{-8}$ , respectively. The training process undergoes  $2 \times 10^6$  steps in total. Further computational details can be found in the Supplementary Information (SI).

## Deep NN Molecular Dynamics

After we have obtained different deep NNFF for liquid water trained with subsets of our DFT training data-set, we can then perform deep NN Molecular Dynamics (NN MD) using the LAMMPS simulation package<sup>65</sup> and the DeepMD plugin.<sup>8</sup> In this way, we can investigate the effects of the training data set size on the convergence of physical properties of water.

Simulations of water at different temperatures  $T$  and pressures  $P$  were performed to investigate the density convergence as a function of the training set size. These systems were first equilibrated over 50 ps by performing an isothermal-isobaric (NPT) simulations (using Nose-Hoover thermostat and barostat<sup>65</sup>). The equilibrium densities were then obtained averaging over 2 ns.

We also carried out NVT simulations of bulk water (512 molecules), controlling the temperature via a stochastic velocity rescaling thermostat.<sup>66</sup> These large systems were equilibrated over 150 ps and then additionally 2 ns simulations were carried out at the production stage.

## Results and discussion

In order to illustrate the performance of our deep NN potential, we show in Figure 1 the parity graphs for the (a) energy and (b) force components. In this particular case, we tested our model on the test set (10% of DFT data reference) and also on the training set itself (90% of DFT data reference), which shows that the NN operates well on both data sets with roughly similar errors, that is a good feature to indicate that the fitted NN is neither under-fitting nor over-fitting.<sup>8</sup>

In particular, we find that the RMSEs (Root Mean Squared Errors) on the test set are  $\sim 46$  meV/Å (force) and  $\sim 0.53$  meV/atom (energy). As recently pointed out by Wen and collaborators<sup>6</sup> the RMSE for forces and energy for a good (high accuracy) deep potential should be of the order of  $< 50$  meV/Å and  $\sim 1$  meV/atom, respectively.

We performed a k-fold cross-validation procedure (see SI for technical details), where our DFT reference data (18,000 snapshots) were separated into 10 subsets of equal size. We then trained/tested different models with different training subsets, while keeping the proportion of

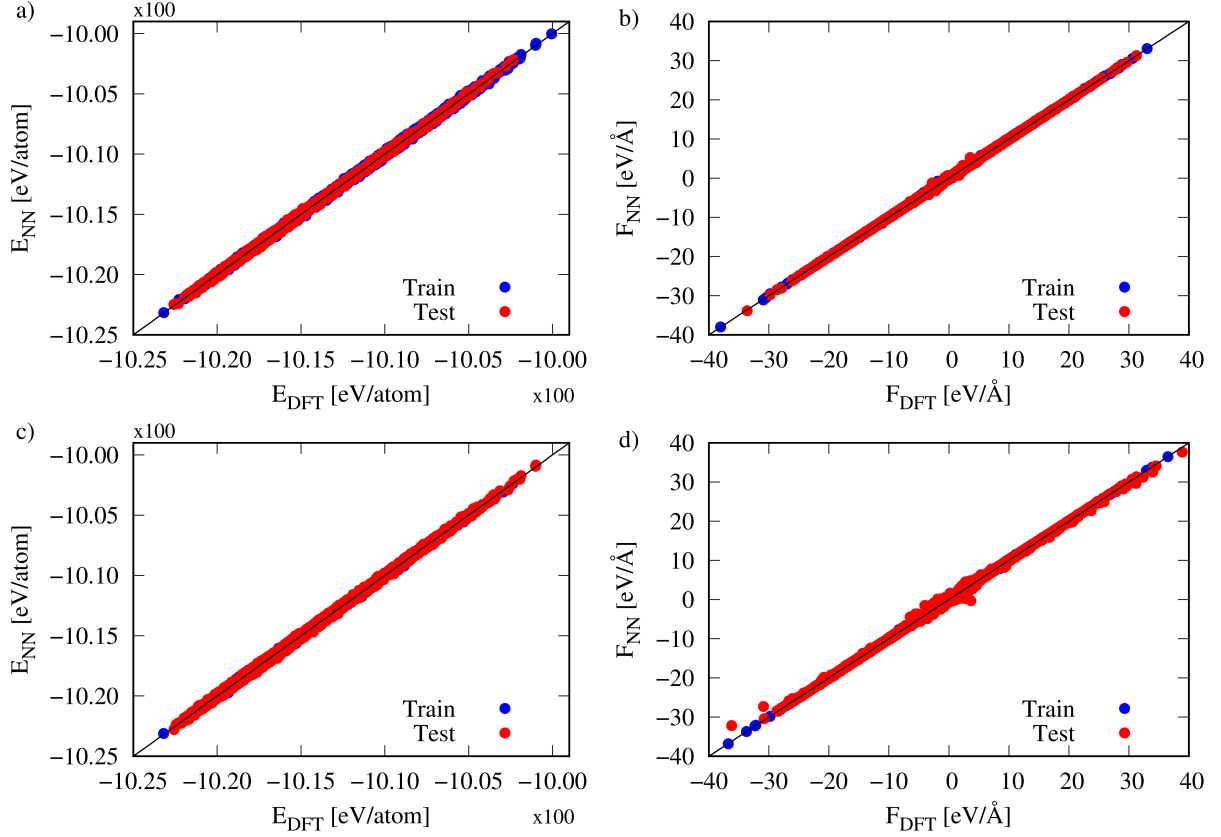


Figure 1: Parity graphs for energy and forces evaluated on the training and test data sets, where a) and b) refer to the 100% case while c) and b) to the case of 10%. The  $E_{NN}$  and  $F_{NN}$  are the NN predicted energy and force, respectively. The DFT data reference are represented by  $E_{DFT}$  and  $F_{DFT}$ .

90% for training and 10% for testing. We show in SI the RMSEs obtained (Table I- SI). We find that the testing errors do not change considerably with different training subsets, and the average of RMSE errors for energy and forces are equal to 0.533 meV/atom and 46.6 meV/Å, respectively. The deviations are in the order of 0.002% (energy) and 0.12% (force), which represents that the DFT reference data are uncorrelated.

In other words, the cross-validation tell us that the trained NNFF does not depend on a particular partition of the DFT data-set. Thus, we can train different NN using a randomly selected subset of the training data set. To exemplify it, we show in Figure 1 c) and d) the parity graphs for the 10% case (1620 randomly selected snapshots used to train a deep NNFF), which shows that this NNFF also performs well on both the testing and training data-sets. In this way, we show in Figure 2 the RMSE and MAE (Mean Absolute Error) for energy (top panel) and force (bottom panel) as a function of the training data set size.

As we can see in Figure 2, the four curves show an initial decrease in error values, after the size of the data-set has reached 20%, they become essentially constant. However, it should be mentioned that even the 10% case is within the accuracy reported in the literature.<sup>6</sup>

Nonetheless, the observation only based on the errors evaluated on test data sets are not enough to affirm that the NNFF will work for a long MD simulation. For example, we considered a different case, where the NNFF was built with correlated data obtained from a 330 K NVT AIMD simulation with van der Waals exchange–correlation functional (vdW-BH<sup>67</sup>). In this case, the training data set has a size similar to the 50% uncorrelated case presented in Figure 2. Although we found the RMSE errors on test data-set smaller than those presented in Figure 2, we can not simulate bulk water for a long time; the energy is only conserved up to  $\sim 20$  ps, after that the system makes non-physical bonds between the atoms and the energy is no longer conserved. See SI for further details.

On the other hand, the deep NNFF trained with only uncorrelated 1620 frames (10% case) allows one to simulate water systems for long times, which shows that correct phase sampling is more important than just the amount of data used in the training process. For example in Table 1,



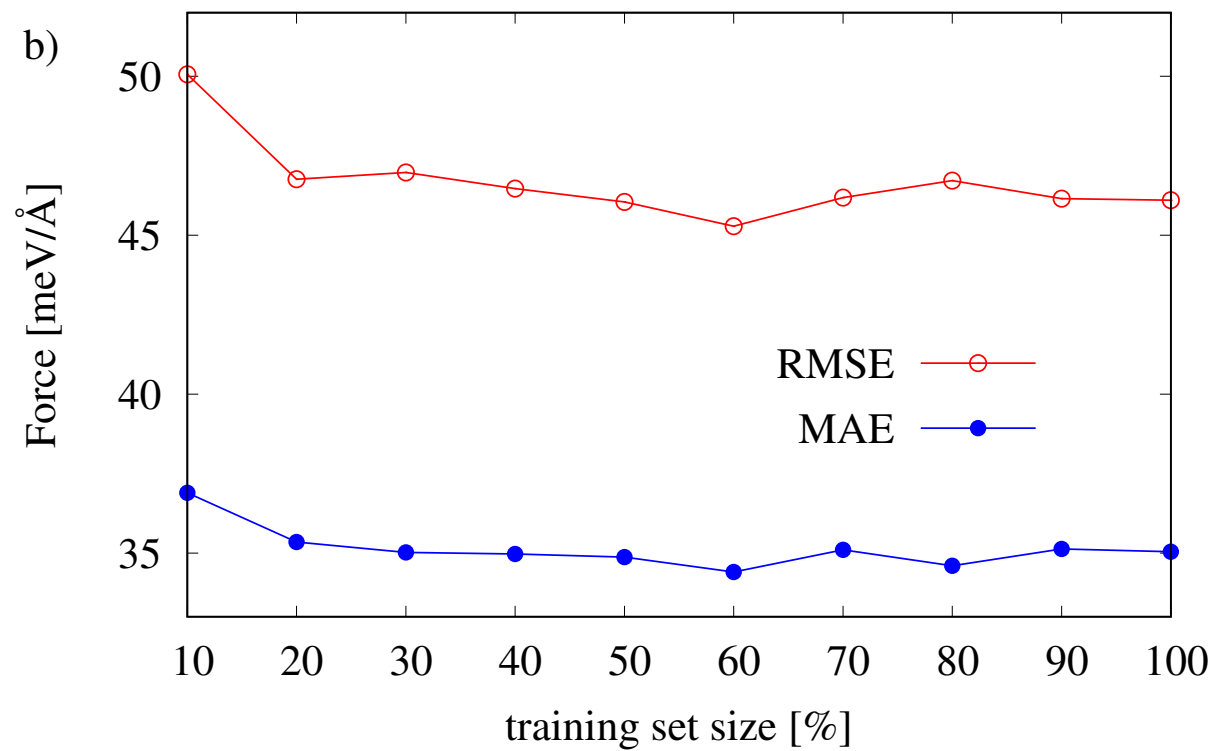
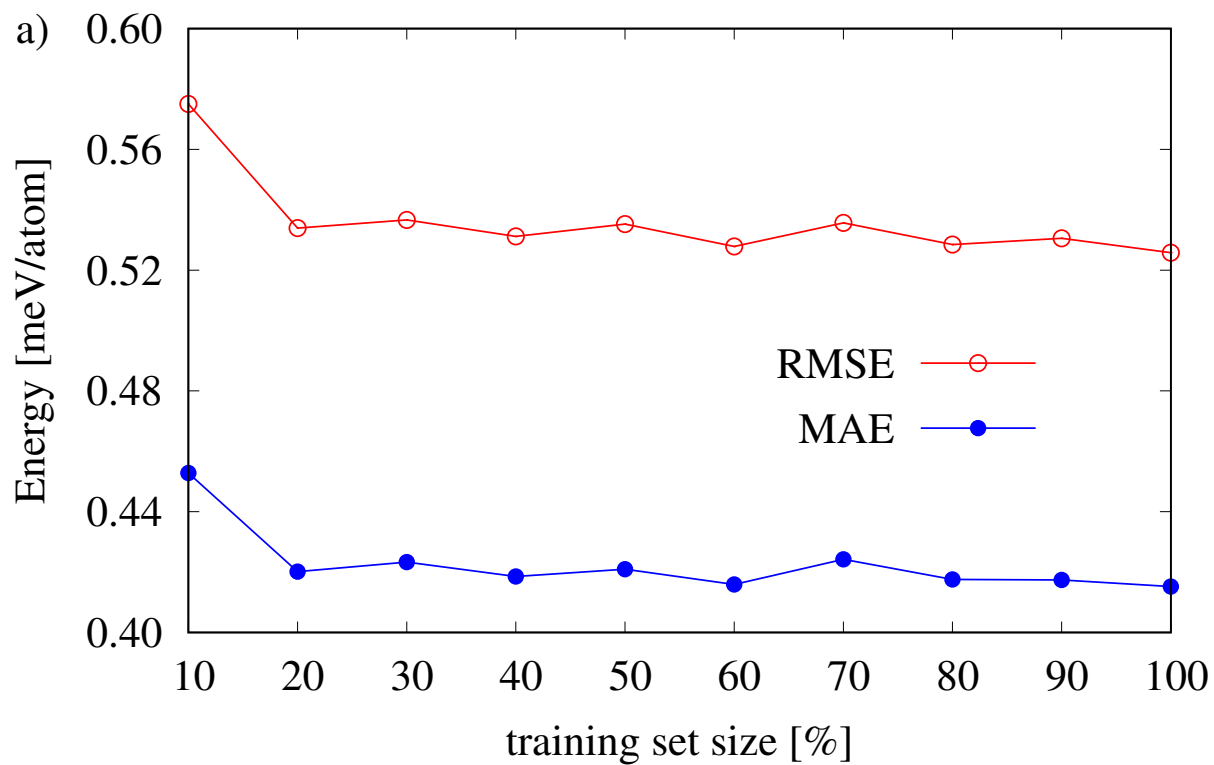


Figure 2: RMSE and MAE for energy (top panel) and forces (bottom panel) as a function of the training set size.

we show the equilibrium water densities,  $\rho_{eq}$ , obtained at different temperatures and at fixed ambient pressure for the 10% and 100% cases. We also show the result for the hexagonal ice  $I_h$  with 96  $H_2O$  at  $T = 273$  K and  $P = 1$  Bar.

Table 1: Equilibrium densities,  $\rho_{eq}$ , for liquid water with 128  $H_2O$  at pressure equal to 1 Bar and temperature equal to 300 K and 350 K. We also show the density result for ice  $I_h$  with 96  $H_2O$  at  $T = 273$  K and  $P = 1$  Bar.

	10%	100%
	$\rho_{eq}$ [g/cm <sup>3</sup> ]	$\rho_{eq}$ [g/cm <sup>3</sup> ]
water: T = 300K	1.015	1.013
water: T = 350K	1.020	1.024
ice $I_h$ : T = 273K	0.957	0.961

It is worth mentioning that for liquid water both NNFFs result in densities with the same precision although one was trained with 1620 samples and another one with ten times more data points. Moreover, it also captures the ice  $I_h$  density in reasonable agreement with other SCAN results under similar thermodynamic conditions (AIMD:<sup>50</sup>  $0.964 \pm 0.023$ ; SCAN DFT<sup>55</sup>  $0.957 \pm 0.004$ ; NNFF<sup>55</sup>  $0.949 \pm 0.001$ ).

Another interesting point is that although our DFT data reference was obtained for liquid water at different temperatures and densities, the NNFF were able to estimate the ice density. In fact, the capability of a ML potential trained on liquid water alone predicting the properties of the ice phases was also recently reported by Monserrat et al.<sup>32</sup>

In Figure 3 we show the pair correlation functions for oxygen–oxygen ( $g_{OO}$ ), oxygen–hydrogen ( $g_{OH}$ ) and hydrogen–hydrogen ( $g_{HH}$ ), which are the main structural descriptors for water.<sup>68–70</sup> These results were obtained for liquid water composed by 512 molecules at fixed density ( $\rho = 0.997$  g/cm<sup>3</sup>) and temperature ( $T = 300$  K). We also show the AIMD results for the SCAN functional for 55 water molecules at the same temperature recently presented by Yao and Kanai.<sup>53</sup> As it can be seen, all results are very similar.

For a better comparison between the NNFF, we measured the relative error between the radial oxygen-oxygen distribution function for each trained NNFF with respect to the hundred percent case, as it is shown in Figure 4. Note that the errors are roughly the same, fluctuating around zero

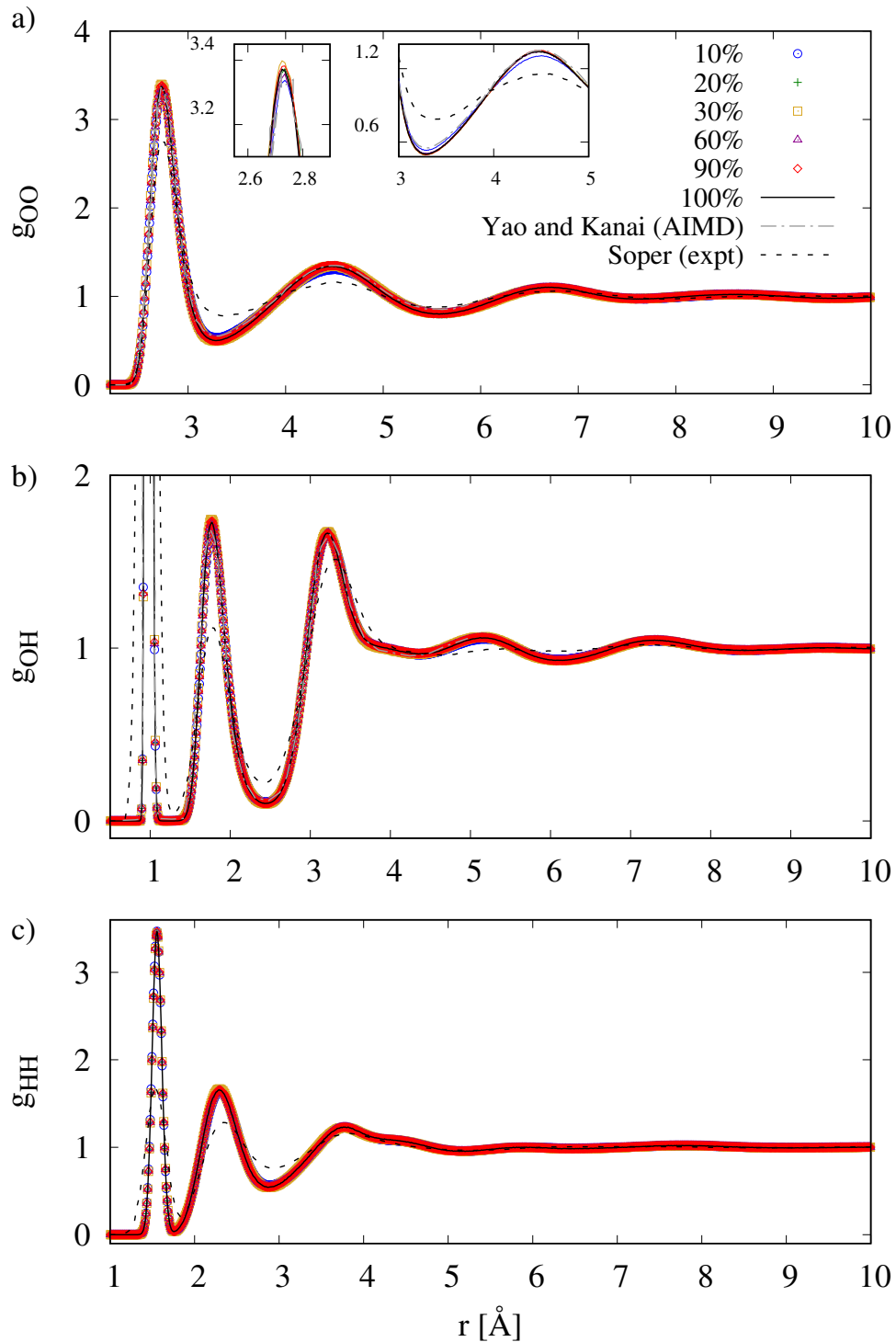


Figure 3: Radial distribution function for (a) O-O, (b) O-H and (c) H-H pairs obtained via NNMD. Each percentage presented refers to the fraction of the original data set used for training. The  $g_{OO}$  and  $g_{OH}$  results<sup>53</sup> obtained from AIMD-based on SCAN functional for 55 water molecules at  $T = 300$  K are represented by dashed lines. The insets in  $g_{OO}$  panel show the points of the first and second peaks. The experimental results from Soper<sup>68</sup> are also shown.

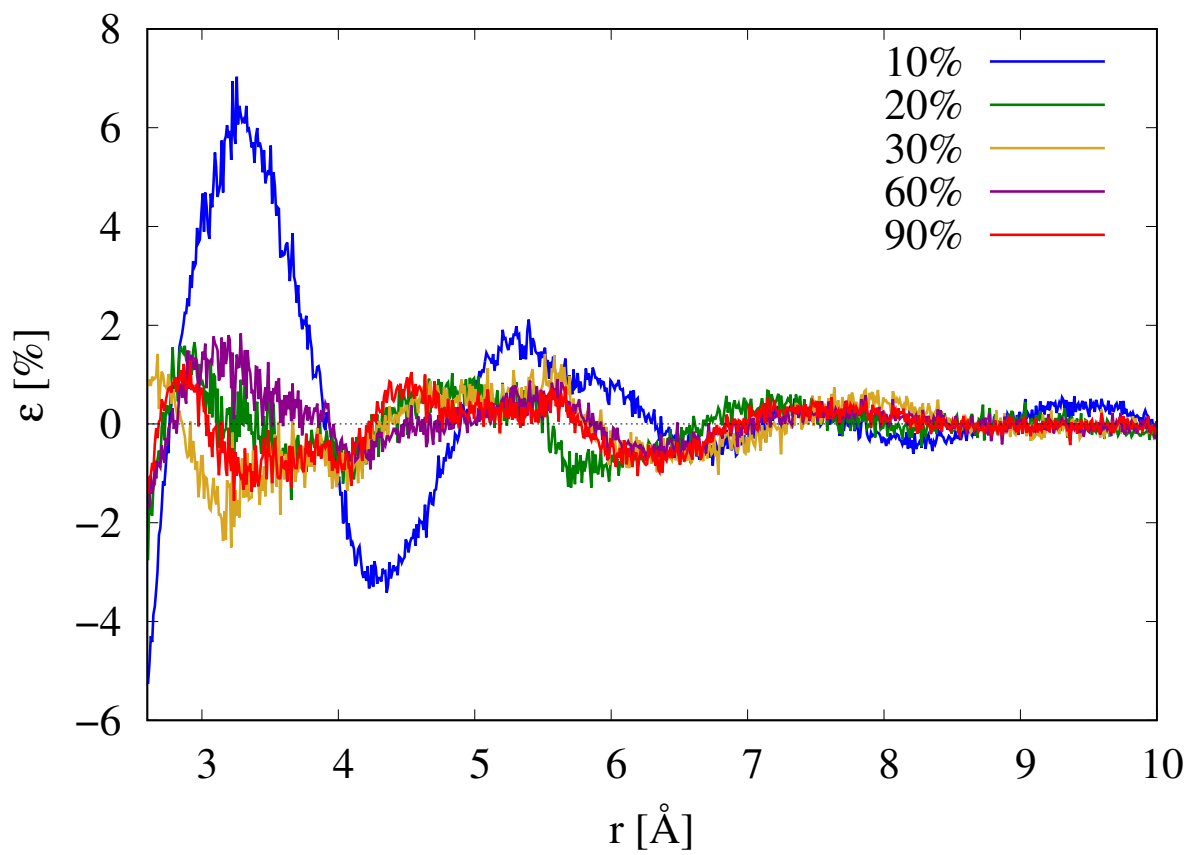


Figure 4: The relative error, of the O-O radial distribution function for different data set sizes, as a function of the distance,  $r$ , in angstrom.

(approximately 2% of error). The only exception is the 10% case that presents errors of  $\sim 6\%$  in the range of  $3 < r < 5 \text{ \AA}$ .

Furthermore, we also analyzed the vibrational spectra obtained from different molecular dynamics simulations (deep NNFF trained with 10% and 100% of the training data-set). All of them have approximately the same pattern, which means that the results for the structural and vibrational properties of bulk water are mostly independent of the size of the training data-set employed to build deep NNFF for liquid water, as long as they have been well chosen.

More importantly, since MD simulations can now be performed for a long time scale, we can investigate the dynamical properties as a function of time. An important feature of bulk water that is not usually well described by AIMD is its self-diffusion coefficient.<sup>26</sup> In fact, the self-diffusion coefficient can depend on many factors even when obtained from a classical MD simulation.<sup>16,71</sup> In Figure 5 we show the self-diffusion coefficient as a function of simulation time, where it was obtained from the Einstein equation of the mean square displacements of the center of mass of water molecules. For further technical details see Ref.<sup>26</sup> As it can be seen, as the time increases the fluctuations are reduced and the value of  $D$  converges. As already shown, this only occurs after 2 ns, way above conventional AIMD capabilities. At a final time (2000 ps), the 10% case is the only one that presents a higher deviation with respect to the 100%.

It should be mentioned that in earlier works,<sup>5,8</sup> the training data-set used to build the ML force fields typically came from AIMD simulations. For example, the data obtained for short simulation time ( $\sim 20$  ps), resulted in a total of  $40 \times 10^3$  correlated configurations.<sup>8</sup> On the other hand, more recently active learning procedures have allowed for the construction of a ML potential with fewer training data points.<sup>7</sup> In the work of Malosso *et al.*, for example, the ML potential for liquid water was trained with 4000 configurations,<sup>56</sup> which is in agreement with the size of the training data-set required for the convergence of the self-diffusion coefficient present in Figure 5. Thus, it is possible that combining uncorrelated snapshots and active learning the size of the data set could be reduced even further.

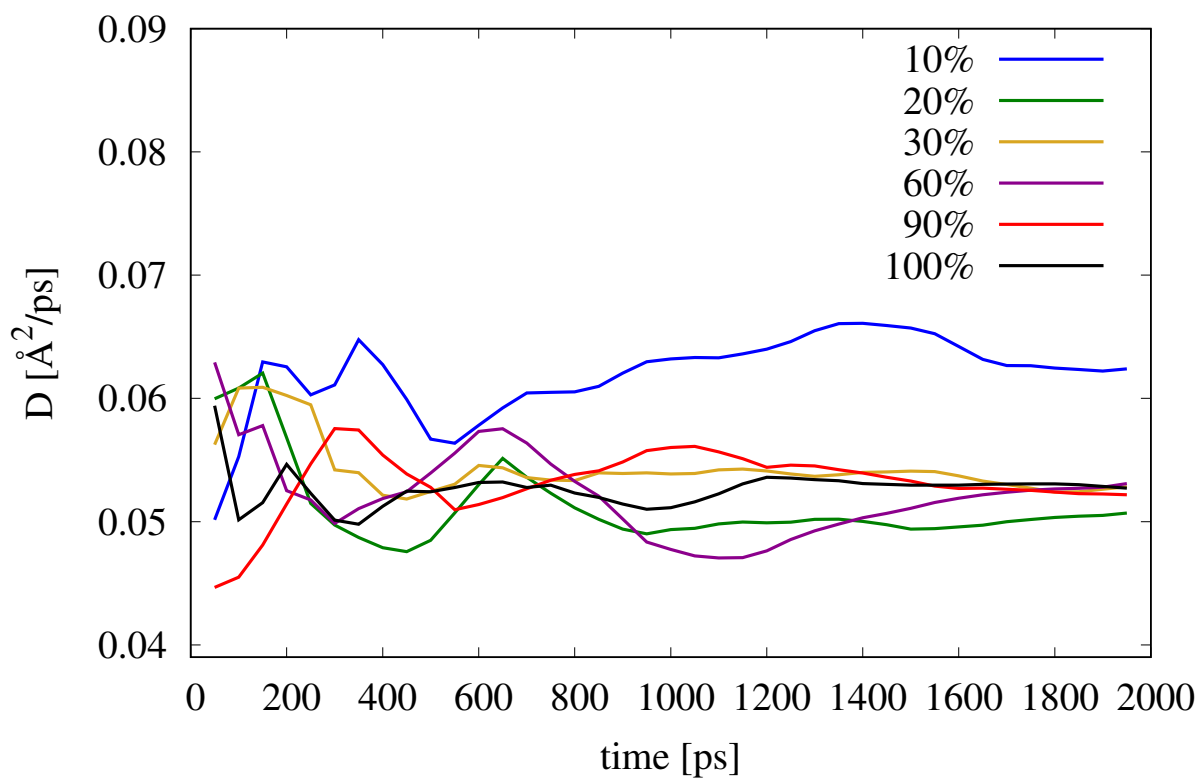


Figure 5: Self-diffusion coefficient as a function of simulation time, for 512 water molecules at  $T = 300$  K and  $\rho = 0.997$  g/cm<sup>3</sup>.

## Conclusions

In this work we analyzed deep neural network potentials for liquid water/ice  $I_h$  based on the SCAN xc-functional.<sup>49</sup> We show that the structural properties such as the equilibrium densities at different temperature and pressures for water are quite independent of the size of the training data-set considered, as the minimum amount employed here was the energy and forces of 1620 structures (64  $H_2O$ ). This quantity is much smaller than what is typically used in the training of other NN. This can be attributed to the method of selecting the snapshots for training, which provide a breadth of structures that best samples the phase space. In this way, we have found that the density, vibrational spectra and the radial distribution function of water are less dependent on the size of the training data-set compared to dynamical ones (e.g, the diffusion coefficient.) Finally, we envision that uncorrelated physical inspired training data-set procedure proposed here (sets that include a broad range of short and long OH bonds) together with active learning, can be a way to produce reliable ML potentials constructed with fewer DFT training data points.

## Supporting Information Available

The Supplementary Information is available free of charge at xxxxx.

- Supplementary information contents: training details, cross-validation, molecular dynamics results, and correlated data.

## Acknowledgement

We acknowledge fruitful discussions with Gabriel C. Santucci and Lucas T. S. de Miranda. The authors acknowledge financial support from FAPESP (Grant # FAPESP 2017/10292-0, 2020/09011-9, 2017/02317-2 and 2016/01343-7). This work used the computational resources from the Centro Nacional de Processamento de Alto Desempenho em São Paulo (CENAPAD-SP) and GRID-UNESP.

## References

- (1) Brooks, C. L.; Case, D. A.; Plimpton, S.; Roux, B.; van der Spoel, D.; Tajkhorshid, E. Classical molecular dynamics. *The Journal of Chemical Physics* **2021**, *154*, 100401.
- (2) Hollingsworth, S. A.; Dror, R. O. Molecular Dynamics Simulation for All. *Neuron* **2018**, *99*, 1129–1143.
- (3) Sethi, S. K.; Kadian, S.; Manik, G. A Review of Recent Progress in Molecular Dynamics and Coarse-Grain Simulations Assisted Understanding of Wettability. *Archives of Computational Methods in Engineering* **2022**, *29*, 3059–3085.
- (4) Batzner, S.; Musaelian, A.; Sun, L.; Geiger, M.; Mailoa, J. P.; Kornbluth, M.; Molinari, N.; Smidt, T. E.; Kozinsky, B. E (3)-equivariant graph neural networks for data-efficient and accurate interatomic potentials. *Nature communications* **2022**, *13*, 1–11.
- (5) Zhang, L.; Han, J.; Wang, H.; Car, R.; E, W. Deep Potential Molecular Dynamics: A Scalable Model with the Accuracy of Quantum Mechanics. *Phys. Rev. Lett.* **2018**, *120*, 143001.
- (6) Wen, T.; Zhang, L.; Wang, H.; E, W.; Srolovitz, D. J. Deep potentials for materials science. *Materials Futures* **2022**, *1*, 022601.
- (7) Zhang, L.; Lin, D.-Y.; Wang, H.; Car, R.; E, W. Active learning of uniformly accurate interatomic potentials for materials simulation. *Phys. Rev. Materials* **2019**, *3*, 023804.
- (8) Wang, H.; Zhang, L.; Han, J.; E, W. DeePMD-kit: A deep learning package for many-body potential energy representation and molecular dynamics. *Computer Physics Communications* **2018**, *228*, 178–184.
- (9) Behler, J. Atom-centered symmetry functions for constructing high-dimensional neural network potentials. *The Journal of Chemical Physics* **2011**, *134*, 074106.
- (10) Pedroza, L. S.; da Silva, A. J. R. Adiabatic intramolecular movements for water systems. *The Journal of Chemical Physics* **2008**, *128*, 104311.



- (11) Jones, J. E. On the Determination of Molecular Fields. I. From the Variation of the Viscosity of a Gas with Temperature. *Proceedings of The Royal Society A: Mathematical, Physical and Engineering Sciences* **1924**, *106*, 441–462.
- (12) Unke, O. T.; Chmiela, S.; Sauceda, H. E.; Gastegger, M.; Poltavsky, I.; Schütt, K. T.; Tkatchenko, A.; Müller, K.-R. Machine Learning Force Fields. *Chemical Reviews* **2021**, *121*, 10142–10186, PMID: 33705118.
- (13) Babin, V.; Leforestier, C.; Paesani, F. Development of a “first principles” water potential with flexible monomers: Dimer potential energy surface, VRT spectrum, and second virial coefficient. *Journal of chemical theory and computation* **2013**, *9*, 5395–5403.
- (14) Babin, V.; Medders, G. R.; Paesani, F. Development of a “first principles” water potential with flexible monomers. II: Trimer potential energy surface, third virial coefficient, and small clusters. *Journal of chemical theory and computation* **2014**, *10*, 1599–1607.
- (15) Medders, G. R.; Babin, V.; Paesani, F. Development of a “first-principles” water potential with flexible monomers. III. Liquid phase properties. *Journal of chemical theory and computation* **2014**, *10*, 2906–2910.
- (16) Kadaoluwa Pathirannahalage, S. P.; Meftahi, N.; Elbourne, A.; Weiss, A. C.; McConville, C. F.; Padua, A.; Winkler, D. A.; Costa Gomes, M.; Greaves, T. L.; Le, T. C., et al. Systematic comparison of the structural and dynamic properties of commonly used water models for molecular dynamics simulations. *Journal of Chemical Information and Modeling* **2021**, *61*, 4521–4536.
- (17) Brini, E.; Fennell, C. J.; Fernandez-Serra, M.; Hribar-Lee, B.; Luksic, M.; Dill, K. A. How water’s properties are encoded in its molecular structure and energies. *Chemical reviews* **2017**, *117*, 12385–12414.
- (18) Car, R.; Parrinello, M. Unified Approach for Molecular Dynamics and Density-Functional Theory. *Phys. Rev. Lett.* **1985**, *55*, 2471–2474.

- (19) Gillan, M. J.; Alfè, D.; Michaelides, A. Perspective: How good is DFT for water? *The Journal of Chemical Physics* **2016**, *144*, 130901.
- (20) Lin, I.-C.; Seitsonen, A. P.; Coutinho-Neto, M. D.; Tavernelli, I.; Rothlisberger, U. Importance of van der Waals interactions in liquid water. *The Journal of Physical Chemistry B* **2009**, *113*, 1127–1131.
- (21) Ruiz Pestana, L.; Marsalek, O.; Markland, T. E.; Head-Gordon, T. The quest for accurate liquid water properties from first principles. *The journal of physical chemistry letters* **2018**, *9*, 5009–5016.
- (22) Waters, J. M., Michael J Rondinelli Benchmarking structural evolution methods for training of machine learned interatomic potentials. *Journal of Physics: Condens. Matter* **2022**, *34*, 385901.
- (23) Friederich, P.; Häse, F.; Proppe, J.; Aspuru-Guzik, A. Machine-learned potentials for next-generation matter simulations. *Nature Materials* **2021**, *20*, 750–761.
- (24) Kocer, E.; Ko, T. W.; Behler, J. Neural Network Potentials: A Concise Overview of Methods. *Annual Review of Physical Chemistry* **2022**, *73*, 163–186.
- (25) Behler, J. First principles neural network potentials for reactive simulations of large molecular and condensed systems. *Angewandte Chemie International Edition* **2017**, *56*, 12828–12840.
- (26) Torres, A.; Pedroza, L. S.; Fernandez-Serra, M.; Rocha, A. R. Using Neural Network Force Fields to Ascertain the Quality of Ab Initio Simulations of Liquid Water. *The Journal of Physical Chemistry B* **2021**, *125*, 10772–10778.
- (27) Deringer, V. L.; Caro, M. A.; Csányi, G. Machine learning interatomic potentials as emerging tools for materials science. *Advanced Materials* **2019**, *31*, 1902765.
- (28) Noé, F.; Tkatchenko, A.; Müller, K.-R.; Clementi, C. Machine learning for molecular simulation. *Annual review of physical chemistry* **2020**, *71*, 361–390.

- (29) Ceriotti, M.; Clementi, C.; Anatole von Lilienfeld, O. Introduction: Machine Learning at the Atomic Scale. *Chemical Reviews* **2021**, *121*, 9719–9721, PMID: 34428897.
- (30) Rupp, M.; Tkatchenko, A.; Müller, K.-R.; von Lilienfeld, O. A. Fast and Accurate Modeling of Molecular Atomization Energies with Machine Learning. *Phys. Rev. Lett.* **2012**, *108*, 058301.
- (31) Zhang, L.; Wang, H.; Car, R.; E, W. Phase Diagram of a Deep Potential Water Model. *Phys. Rev. Lett.* **2021**, *126*, 236001.
- (32) Monserrat, B.; Brandenburg, J. G.; Engel, E. A.; Cheng, B. Liquid water contains the building blocks of diverse ice phases. *Nature communications* **2020**, *11*, 1–8.
- (33) Reinhardt, A.; Cheng, B. Quantum-mechanical exploration of the phase diagram of water. *Nature communications* **2021**, *12*, 1–7.
- (34) Schran, C.; Thiemann, F. L.; Rowe, P.; Müller, E. A.; Marsalek, O.; Michaelides, A. Machine learning potentials for complex aqueous systems made simple. *Proceedings of the National Academy of Sciences* **2021**, *118*, e2110077118.
- (35) Blank, T. B.; Brown, S. D.; Calhoun, A. W.; Doren, D. J. Neural network models of potential energy surfaces. *The Journal of Chemical Physics* **1995**, *103*, 4129–4137.
- (36) Behler, J.; Parrinello, M. Generalized Neural-Network Representation of High-Dimensional Potential-Energy Surfaces. *Phys. Rev. Lett.* **2007**, *98*, 146401.
- (37) Schütt, K. T.; Sauceda, H. E.; Kindermans, P.-J.; Tkatchenko, A.; Müller, K.-R. SchNet – A deep learning architecture for molecules and materials. *The Journal of Chemical Physics* **2018**, *148*, 241722.
- (38) Lorenz, S.; Groß, A.; Scheffler, M. Representing high-dimensional potential-energy surfaces for reactions at surfaces by neural networks. *Chemical Physics Letters* **2004**, *395*, 210–215.

- (39) Lot, R.; Pellegrini, F.; Shaidu, Y.; Küçükbenli, E. PANNA: Properties from Artificial Neural Network Architectures. *Computer Physics Communications* **2020**, *256*, 107402.
- (40) Gao, A.; Remsing, R. C. Self-consistent determination of long-range electrostatics in neural network potentials. *Nature communications* **2022**, *13*, 1–11.
- (41) Chmiela, S.; Sauceda, H. E.; Poltavsky, I.; Müller, K.-R.; Tkatchenko, A. sGDML: Constructing accurate and data efficient molecular force fields using machine learning. *Computer Physics Communications* **2019**, *240*, 38–45.
- (42) Bartók, A. P.; Payne, M. C.; Kondor, R.; Csányi, G. Gaussian Approximation Potentials: The Accuracy of Quantum Mechanics, without the Electrons. *Phys. Rev. Lett.* **2010**, *104*, 136403.
- (43) Bartók, A. P.; Csányi, G. Gaussian approximation potentials: A brief tutorial introduction. *International Journal of Quantum Chemistry* **2015**, *115*, 1051–1057.
- (44) Drautz, R. Atomic cluster expansion for accurate and transferable interatomic potentials. *Phys. Rev. B* **2019**, *99*, 014104.
- (45) Schleder, G. R.; Padilha, A. C.; Acosta, C. M.; Costa, M.; Fazzio, A. From DFT to machine learning: recent approaches to materials science—a review. *Journal of Physics: Materials* **2019**, *2*, 032001.
- (46) Schleder, G. R.; Padilha, A. C. M.; Reily Rocha, A.; Dalpian, G. M.; Fazzio, A. Ab Initio Simulations and Materials Chemistry in the Age of Big Data. *Journal of Chemical Information and Modeling* **2020**, *60*, 452–459, PMID: 31651163.
- (47) Butler, K. T.; Davies, D. W.; Cartwright, H.; Isayev, O.; Walsh, A. Machine learning for molecular and materials science. *Nature* **2018**, *559*, 547–555.
- (48) Imbalzano, G.; Anelli, A.; Giofré, D.; Klees, S.; Behler, J.; Ceriotti, M. Automatic selection of atomic fingerprints and reference configurations for machine-learning potentials. *The Journal of chemical physics* **2018**, *148*, 241730.

- (49) Sun, J.; Ruzsinszky, A.; Perdew, J. P. Strongly Constrained and Appropriately Normed Semilocal Density Functional. *Phys. Rev. Lett.* **2015**, *115*, 036402.
- (50) Chen, M.; Ko, H.-Y.; Remsing, R. C.; Andrade, M. F. C.; Santra, B.; Sun, Z.; Selloni, A.; Car, R.; Klein, M. L.; Perdew, J. P.; Wu, X. Ab initio theory and modeling of water. *Proceedings of the National Academy of Sciences* **2017**, *114*, 10846–10851.
- (51) Zheng, L.; Chen, M.; Sun, Z.; Ko, H.-Y.; Santra, B.; Dhruvad, P.; Wu, X. Structural, electronic, and dynamical properties of liquid water by ab initio molecular dynamics based on SCAN functional within the canonical ensemble. *The Journal of Chemical Physics* **2018**, *148*, 164505.
- (52) LaCount, M. D.; Gygi, F. Ensemble first-principles molecular dynamics simulations of water using the SCAN meta-GGA density functional. *The Journal of Chemical Physics* **2019**, *151*, 164101.
- (53) Yao, Y.; Kanai, Y. Temperature dependence of nuclear quantum effects on liquid water via artificial neural network model based on SCAN meta-GGA functional. *The Journal of Chemical Physics* **2020**, *153*, 044114.
- (54) Gartner-III, T. E.; Zhang, L.; Piaggi, P. M.; Car, R.; Panagiotopoulos, A. Z.; Debenedetti, P. G. Signatures of a liquid-liquid transition in an ab initio deep neural network model for water. *Proceedings of the National Academy of Sciences* **2020**, *117*, 26040–26046.
- (55) Piaggi, P. M.; Panagiotopoulos, A. Z.; Debenedetti, P. G.; Car, R. Phase Equilibrium of Water with Hexagonal and Cubic Ice Using the SCAN Functional. *Journal of Chemical Theory and Computation* **2021**, *17*, 3065–3077.
- (56) Malosso, C.; Zhang, L.; Car, R.; Baroni, S.; Tisi, D. Viscosity in water from first-principles and deep-neural-network simulations. *npj Computational Materials* **2022**,

- (57) Hone, T. D.; Rossky, P. J.; Voth, G. A. A comparative study of imaginary time path integral based methods for quantum dynamics. *The Journal of Chemical Physics* **2006**, *124*, 154103.
- (58) Habershon, S.; Markland, T. E.; Manolopoulos, D. E. Competing quantum effects in the dynamics of a flexible water model. *The Journal of Chemical Physics* **2009**, *131*, 024501.
- (59) Virtanen, P. et al. SciPy 1.0: Fundamental Algorithms for Scientific Computing in Python. *Nature Methods* **2020**, *17*, 261–272.
- (60) Kresse, G.; Furthmüller, J. Efficient iterative schemes for ab initio total-energy calculations using a plane-wave basis set. *Phys. Rev. B* **1996**, *54*, 11169–11186.
- (61) Kresse, G.; Joubert, D. From ultrasoft pseudopotentials to the projector augmented-wave method. *Phys. Rev. B* **1999**, *59*, 1758–1775.
- (62) Chollet, F. *Deep learning with Python*; Simon and Schuster, 2021.
- (63) Zhang, L.; Han, J.; Wang, H.; Saidi, W.; Car, R.; E, W. End-to-end Symmetry Preserving Inter-atomic Potential Energy Model for Finite and Extended Systems. *Advances in Neural Information Processing Systems*. 2018.
- (64) Kingma, D. P.; Ba, J. Adam: A Method for Stochastic Optimization. 2014.
- (65) Thompson, A. P.; Aktulga, H. M.; Berger, R.; Bolintineanu, D. S.; Brown, W. M.; Crozier, P. S.; in't Veld, P. J.; Kohlmeyer, A.; Moore, S. G.; Nguyen, T. D., et al. LAMMPS-a flexible simulation tool for particle-based materials modeling at the atomic, meso, and continuum scales. *Computer Physics Communications* **2022**, *271*, 108171.
- (66) Bussi, G.; Zykova-Timan, T.; Parrinello, M. Isothermal-isobaric molecular dynamics using stochastic velocity rescaling. *The Journal of Chemical Physics* **2009**, *130*, 074101.
- (67) Berland, K.; Hyldgaard, P. Exchange functional that tests the robustness of the plasmon description of the van der Waals density functional. *Phys. Rev. B* **2014**, *89*, 035412.

- (68) Soper, A. The radial distribution functions of water and ice from 220 to 673 K and at pressures up to 400 MPa. *Chemical Physics* **2000**, 258, 121–137.
- (69) Soper, A. Determination of the orientational pair correlation function of a molecular liquid from diffraction data. *Journal of Molecular Liquids* **1998**, 78, 179–200.
- (70) Vega, C.; McBride, C.; Sanz, E.; Abascal, J. L. F. Radial distribution functions and densities for the SPC/E, TIP4P and TIP5P models for liquid water and ices Ih, Ic, II, III, IV, V, VI, VII, VIII, IX, XI and XII. *Phys. Chem. Chem. Phys.* **2005**, 7, 1450–1456.
- (71) Tsimpanogiannis, I. N.; Moulton, O. A.; Franco, L. F. M.; de M. Spera, M. B.; Erdős, M.; Economou, I. G. Self-diffusion coefficient of bulk and confined water: a critical review of classical molecular simulation studies. *Molecular Simulation* **2019**, 45, 425–453.

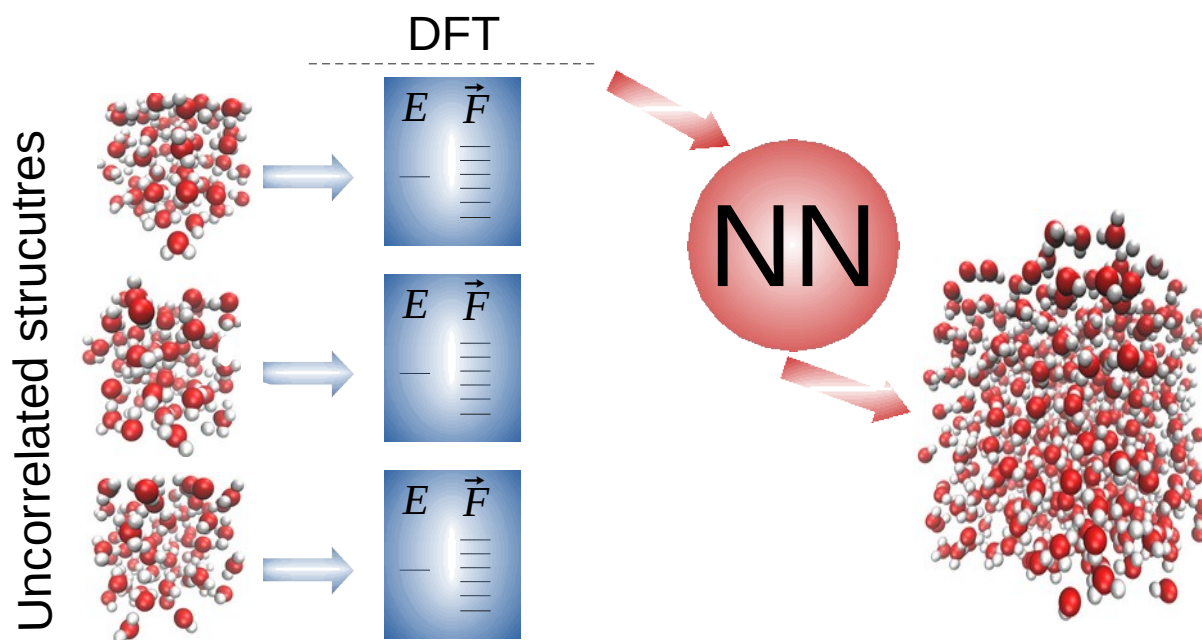


Figure 6: TOC graphic.

# Supporting Information: Size and Quality of Quantum Mechanical Data Sets for Training Neural Network Force Fields for Liquid Water

## SI note 1: Training parameters

We have used the current version of the package DeePMD-kit v2.1.3<sup>1</sup> to generate deep Neural Network Force Fields (NNFF) for bulk water based on the SCAN functional.<sup>2</sup> A different deep-NNFF was obtained for each subset of the training data-set. The DFT data reference employed here were obtained in a previous work<sup>3</sup> (see main text for details on the training data-set).

In particular, we have used the Deep Potential-Smooth Edition descriptor, in which the full relative coordinates are used to build the descriptor. We trained our neural network (NN) using a randomly selected subset of the training data set ranging from 10% to 100% of 16200 samples. We scaled down the NN in order to maintain the total number of fitted parameters and avoid overfitting. For example, the NN topology was chosen to be (32, 16, 4, 2) and (320, 160, 32, 16) for the 10% and 100% case, respectively.

For all trained deep NNFF, we kept fixed the size of the embedding (25,50,100), the cutoff radius (6 Å), and the smoothing parameter was chosen to be equal to 0.50 Å (similar to the NNFF proposed for water by Zhang et al.<sup>4</sup>). The possible maximum number of neighbors in the cut-off radius is set to be 46 and 92 for oxygen and hydrogen atoms, respectively. The flag `axis_neuron` is set to 16, which means that this is the size of submatrix of the embedding matrix, for details see.<sup>5</sup>

The loss function is composed by the mean squared errors of the energies and forces, where its hyper-parameters were chosen to `start_pref_e` = 0.02, `limit_pref_e` = 8, `start_pref_f` = 1500 and `limit_pref_f` = 1.

The loss function was minimized with the Adam stochastic gradient descent method until  $2 \times 10^6$  steps with the starting and stopping learning equal to  $10^{-3}$  and  $3.51 \times 10^{-8}$ , respectively.



## SI note 2: cross-validation

We performed a K-fold cross-validation procedure in order to verify whether the DFT reference data<sup>3</sup> are correlated or not. The K-fold cross-validation essentially consists in partitioning the data set into  $K$  equal parts, then  $K - 1$  partitions are used for training and one is designated for testing,<sup>6,7</sup> as it is illustrated in Figure 7. Note that this process is performed  $K$  times.

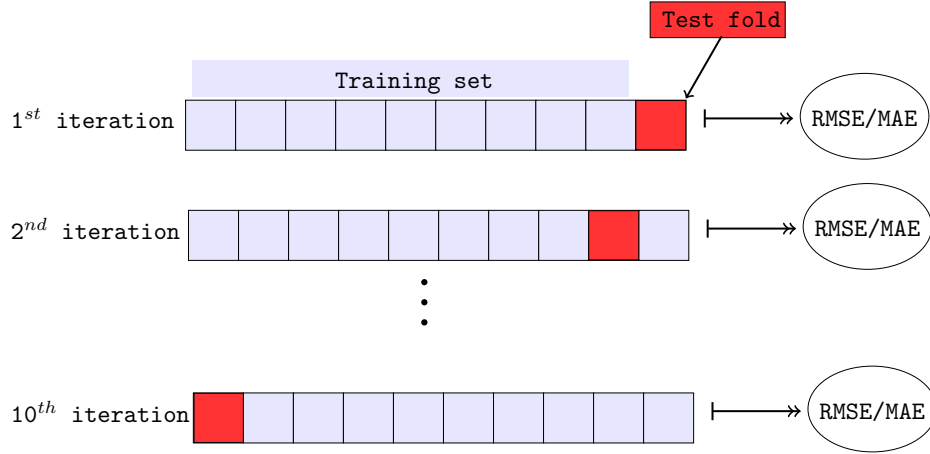


Figure 7: K-fold cross-validation diagram, where  $K = 10$ , i.e 90% of the DFT data reference is used for training process, while the remaining 10% is used for testing. The error (RMSE/MAE) is obtained for each iteration and the final average results are listed in Table 2.

This cross-checking is usually assigned to test the machine learning approaches in situations where the number of data sets is limited.<sup>7</sup> In our case, we used it to verify if the deep neural network potential depends on a particular partition of the DFT data set considered. With respect to NN accuracy, we computed the errors values for both energy and force by MAE (Mean Absolute Error):

$$MAE = \frac{1}{n} \sum_i^n |y_i - \hat{y}_i|, \quad (1)$$

and by RMSE (Root Mean Squared Error):

$$RMSE = \sqrt{\frac{1}{n} \sum_i^n (y_i - \hat{y}_i)^2}, \quad (2)$$

where  $n$  is the number of samples,  $\hat{y}_i$  the DFT reference (energy or force) and  $y_i$  the predicted value.

Table 2: : 10-fold cross-validation: values of the RMSE and MAE on test data-set. All NNs present similar results. The last two lines designate the average and the standard deviation (std) values.

	Energies [eV/atom]		Forces [eV/Å]	
k	RMSE	MAE	RMSE	MAE
1	0.000526	0.000415	0.046102	0.035042
2	0.000524	0.000414	0.045933	0.035076
3	0.000544	0.000431	0.047203	0.036042
4	0.000552	0.000435	0.048040	0.036647
5	0.000516	0.000408	0.045855	0.035020
6	0.000543	0.000426	0.047148	0.036018
7	0.000516	0.000406	0.045123	0.034423
8	0.000522	0.000411	0.045615	0.034856
9	0.000567	0.000447	0.049275	0.037491
10	0.000522	0.000411	0.045811	0.035023
average	0.000533	0.000420	0.046611	0.035564
std	0.000016	0.000013	0.001221	0.000910

We show the RMSE and MAE obtained for each iteration of the 10-fold cross-validation procedure in Table 2, where the last two lines represent the average and its standard deviations (std). Note that each standard deviation is quite small, meaning that testing errors do not change considerably with different training subsets, which means that the DFT reference data are uncorrelated.

## SI note 3: molecular dynamics results

### Structural properties

The results here are for bulk water simulation presented in the main text for a system composed by 512 H<sub>2</sub>O molecules at 300 K. We calculated  $n(r)$ , which is the integral of the radial oxygen-oxygen distribution function,  $g_{OO}(r)$ . This represent the number of oxygen atoms at a given distance  $r$  (coordination number) (shown in Fig. 8).

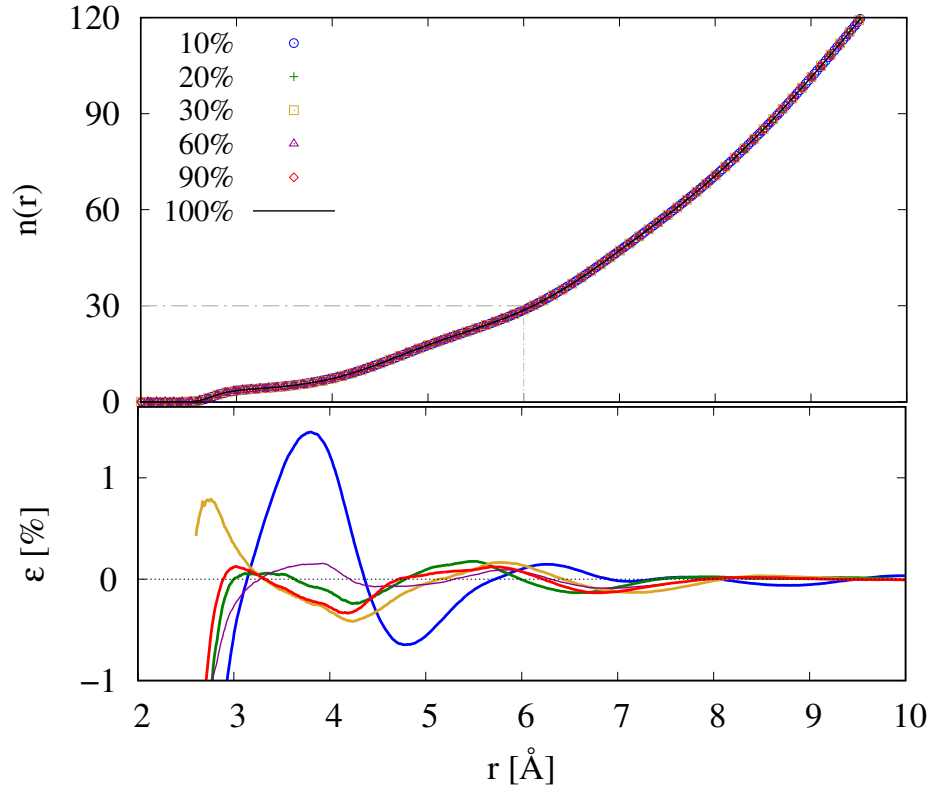


Figure 8: Top to bottom: integration number,  $n(r)$ , as a function of the distance  $r$  in angstrom for the oxygen-oxygen pair; integration of  $g_{OO}(r)$ . The relative error,  $\varepsilon[\%]$ , with respect to the hundred percent case. Each percentage is the quantity of data points used in the training process, for instance, 10% is equivalent to 1620 samples.

We also show the relative error,  $\varepsilon$ , with respect to a hundred percent case,  $\varepsilon = \left( \frac{n(r)^\xi - n(r)^{100}}{n(r)^{100}} \right) \times 100$ , with  $\xi = \{10, 20, 30, 60, 80\}\%$ . As we can see,  $n(r)$  presents a similar behavior for all cases. Furthermore, the vertical dashed line shows that the expected number of water molecules within a sphere of radius equal to 6 Å was correctly obtained for all deep NNFF. The relative error shows that the errors are roughly the same, fluctuating around zero, exceptions only for the 10% case in the range of  $3 < r < 5$  Å. Therefore, the results for the structural properties of bulk water are quite independent on the size of the training data set.

## Vibrational spectra

We show in Figure 9 the vibrational spectra of liquid water, which was obtained by the Fourier transform of the velocity autocorrelation function,<sup>8</sup> i.e,

$$I(\omega) = \frac{1}{2\pi} \int_{-\infty}^{\infty} \langle \vec{v}_i(t) \cdot \vec{v}_i(0) \rangle \exp(i\omega t) dt, \quad (3)$$

where  $\vec{v}_i(t)$  is the velocity of the atom  $i$  at time  $t$  and  $\omega$  is the frequency. As it can be seen, the vibrational spectra obtained from different molecular dynamics simulations (deep NNFF trained with 10% and 100% of the training data-set) have approximately the same pattern, which means that the results of the vibrational properties of bulk water are quite independent of the size of the training data-set employed to built deep NNFF for liquid water.

## SI note 4: correlated data

In order to show that a good sampling (selecting reference data for the training process) is a crucial step to obtain a deep NNFF, we have built a NNFF with the data used for training extracted from a 330 K NVT AIMD simulation with van der Waals exchange–correlation functional, as proposed by Berland and Hyldgaard.<sup>9</sup> The data set was generated by simulating a bulk liquid water system of 64 molecules using the SIESTA package.<sup>10</sup> The time step was 0.50 fs and the total number of

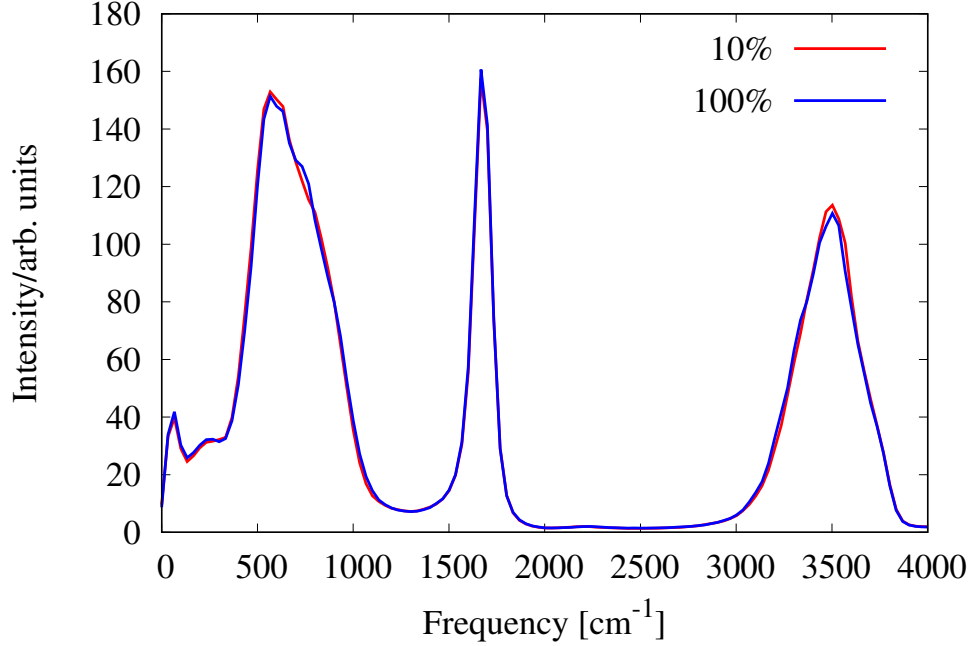


Figure 9: The vibrational spectra of liquid water (512 H<sub>2</sub>O at T = 300K) obtained by the Fourier transform of velocity autocorrelation function, equation (3).

steps set up to  $10^4$ .

For training process, we discarded the first 500 frames and the 9500 frames was randomly shuffled. We then selected 90% of the data-set for training while 10% was used as testing data. Note that this training data set has size similar to our 50% uncorrelated case presented in the main text. Thus, we adopted the same training parameters as used in the 50% case, for example, the number of hidden layers is 4, the number of neurons in each layer is set to (160, 80, 16, 8).

In figure 10, we show that the deep NNFF present good accuracy on both training and test data sets. The RMSE error values are listed in table 3. Also note that these errors are smaller than those obtained from the 50% uncorrelated case (see Fig 2 in the main text).

However, the evaluation of errors on the test data set is not enough to ensure that a good NNFF for liquid water was achieved. For instance, when we performed a simulation for a large system and for long simulation time (similar to the simulation for the bulk water presented in the main text), the energy is only conserved up to  $\sim 20$  ps of simulation time, after that the system makes non-physical bonds between the atoms and the energy is no longer conserved. In Figure 11 we

show the pair correlation functions for oxygen–oxygen ( $g_{OO}$ ) obtained via AIMD (64  $\text{H}_2\text{O}$ ) and via NNMD (512  $\text{H}_2\text{O}$ ) for a total of 20 ps and 30 ps.

Therefore, it should be noted that we were able to simulate for long times the same system with a deep NNFF trained with only 1620 frames (10% case), showing that correct phase space sampling is more important than just the quantity of data used in the training process.

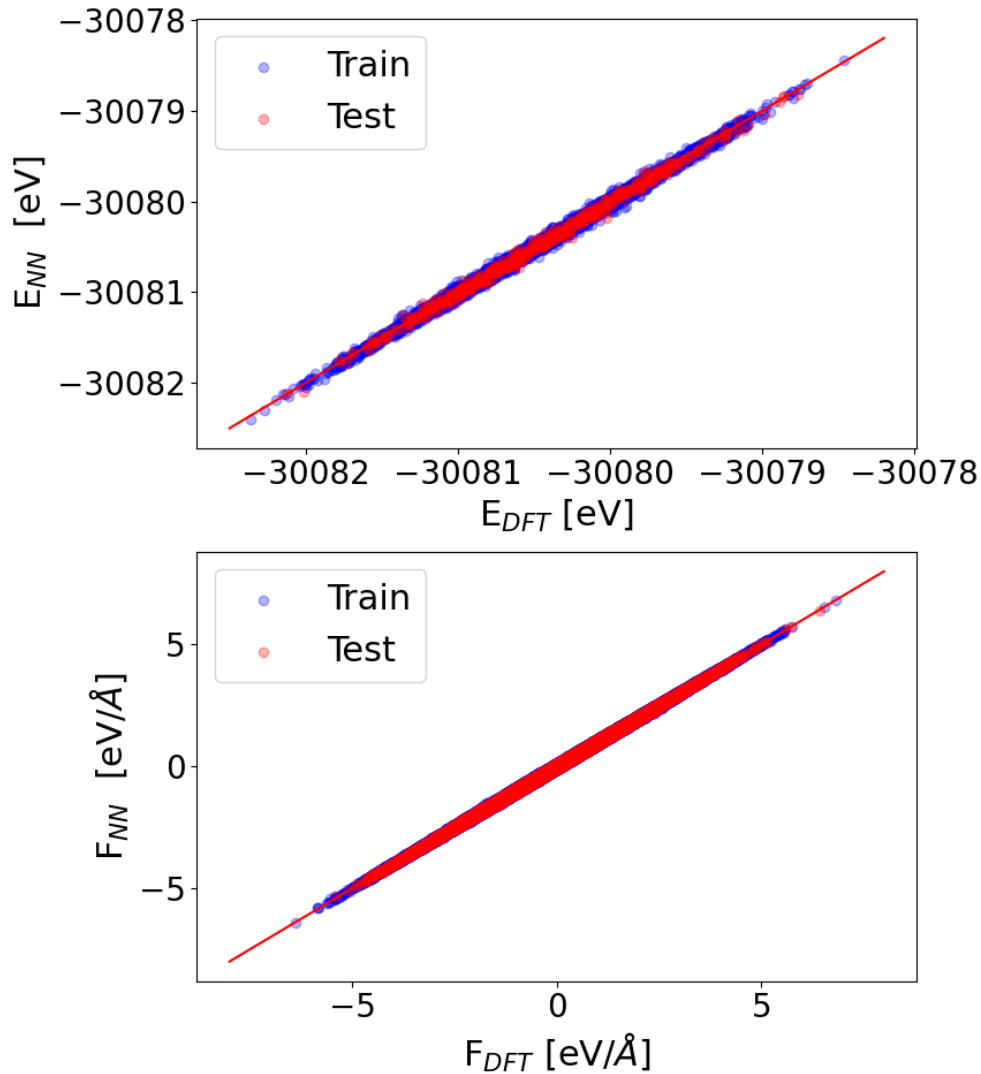


Figure 10: Parity graphs for energy and forces evaluated on the training and testing data sets. The  $E_{NN}$  and  $F_{NN}$  are the NN predicted energy and force, respectively. Already the DFT data reference are represented by  $E_{DFT}$  and  $F_{DFT}$ .

Table 3: Neural network RMSE errors on the training and test sets.

	Test	Train
Energies [meV/atom]	0.199	0.192
Forces [meV/Å]	29.28	28.99

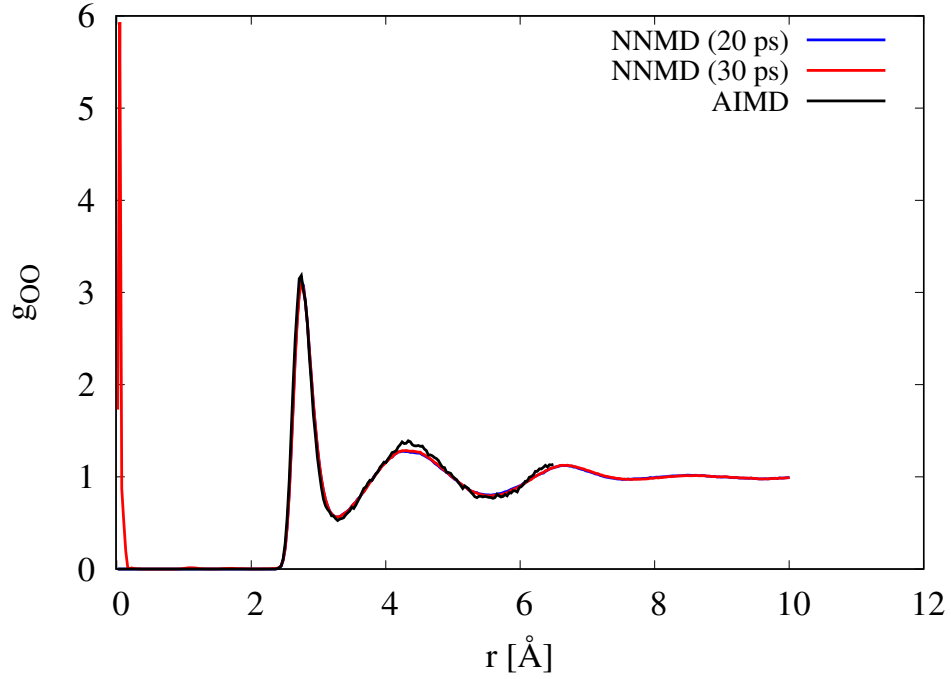


Figure 11: Radial distribution function for O-O obtained via AIMD (64 H<sub>2</sub>O for 5 ps) and via NNMD (512 H<sub>2</sub>O) for a total of 20 ps and 30 ps.

## References

- (1) H. Wang, L. Zhang, J. Han, and E. Weinan, *Computer Physics Communications*, **228**, 178-184 (2018).
- (2) J. Sun, A. Ruzsinszky, and J. P. Perdew, *Physical Review Letters* **115**, 036402 (2015).
- (3) A. Torres, L. S. Pedroza, M. Fernandez-Serra, and A. R. Rocha, *The Journal of Physical Chemistry B* **125**, 10772–10778 (2021).
- (4) L. Zhang, H. Wang, R. Car, and E. Weinan, *Physical Review Letters* **126**, 236001 (2021).
- (5) DeepModeling <https://deepmodeling.com/>
- (6) F. Chollet, *Deep learning with Python* (Simon and Schuster, 2021).
- (7) R. Schleder, A. C. Padilha, C. M. Acosta, M. Costa, and A. Fazzio, *Journal of Physics: Materials* **3**, 032001 (2019).
- (8) Allen, Michael P., and Dominic J. Tildesley. *Computer simulation of liquids*. Oxford university press, 2017.
- (9) K. Berland and P. Hyldgaard, *Phys. Rev. B* **89**, 035412 (2014).
- (10) J. M. Soler, E. Artacho, J. D. Gale, A. García, J. Junquera, P. Ordejón, and D. Sánchez-Portal, *Journal of Physics: Condensed Matter* **14** 2745 (2002).